Noiseless linear amplification and loss-tolerant quantum relay using coherent-state superpositions

Joshua J. Guanzon,[1,*] Matthew S. Winnel,[1] Austin P. Lund,[2,1] and Timothy C. Ralph[1]
[1]*Centre for Quantum Computation and Communication Technology, School of Mathematics and Physics, The University of Queensland, St Lucia, Queensland 4072, Australia*
[2]*Dahlem Center for Complex Quantum Systems, Freie Universität Berlin, 14195 Berlin, Germany*

(Received 22 November 2022; revised 3 June 2023; accepted 22 August 2023; published 12 September 2023)

Noiseless linear amplification (NLA) is useful for a wide variety of quantum protocols. Here we propose a fully scalable amplifier which, for asymptotically large sizes, can perform perfect fidelity NLA on any quantum state. Given finite resources, however, it is designed to perform perfect fidelity NLA on coherent states and their arbitrary superpositions. Our scheme is a generalization of the multiphoton quantum scissor teleamplifier, which we implement using a coherent-state superposition resource state. Furthermore, we prove our NLA is also a loss-tolerant relay for multiary phase-shift keyed coherent states. Finally, we demonstrate that our NLA is also useful for continuous-variable entanglement distillation, even with realistic experimental imperfections.

DOI: 10.1103/PhysRevA.108.032411

I. INTRODUCTION

Coherent states, which can be approximated by laser light, already exhibit favorable quantum properties such as minimum uncertainty. It follows naturally that the ability to control an arbitrary superposition of coherent states would be powerful for a wide range of quantum protocols, such as for quantum computing [1–5], quantum metrology [6–10], and quantum communication [11–14].

One type of control which is essential for many quantum protocols is *amplification*, which increases the average number of photons. This could be done in a variety of different ways [15–22], however, an amplifier is more useful for quantum protocols if it satisfies two properties. First, the amplifier is *linear*, where it preserves phase relations and thus arbitrary superposition of the input state. Second, the amplifier is *noiseless*, where it does not add any additional noise in comparison to the input state. This is especially important for a superposition of coherent states, which are known to be susceptible to losing their quantum interference fringes [23,24]. Therefore, *noiseless linear amplification* (NLA) produces the best quality amplified states, with the downside that in general this process must be probabilistic due to the no-cloning theorem [25].

A particular well-studied subset of coherent-state superpositions is the cat state, which is an equal superposition of coherent states, and whose name is in reference to Schrödinger's cat thought experiment [26]. There are numerous known methods for generating high-quality cat states [27–31]. These cat states can then be used as a resource for NLA of an arbitrary superposition of coherent states, based on the procedure given in Ref. [32]. This process works by teleporting the input state onto a resource state, hence it is also known as teleamplification. This is an example of perfect fidelity NLA of a continuous-variable (CV) superposition state, using finite resources. More precisely, suppose we have a resource cat state with N components, where N is the number of coherent states in the superposition. We can use this teleamplifier to perform NLA on any arbitrary superposition state containing up to N components. If applied to an input alphabet containing only coherent states, the teleamplifier still operates well in the presence of large losses, i.e., for use as an untrusted quantum repeater or relay; this could be useful for quantum key distribution (QKD) via N-ary phase-shift keyed (N-PSK) coherent states [33,34]. However, the results given in Ref. [32] only prove and provide the optical networks required to perform NLA on states with $N = 2$ or 4 components.

In this work, we propose a fully scalable teleamplifier protocol, which can perform perfect fidelity NLA for any integer $N \geqslant 2$, thereby filling in this missing knowledge gap. As an immediate corollary, since any quantum state can be represented in the asymptotic limit of $N \to \infty$ components [35], our protocol can in principle perform NLA on any arbitrary quantum state. Indeed, our proposed device can actually implement the so-called exact immaculate amplification process, first hypothesized in Ref. [36]. The structure of our proposed device is inspired by the multiphoton quantum scissor teleamplifier. The single-photon quantum scissor [37] can perform perfect fidelity NLA on quantum states containing up to a single photon [38]. There were attempts to generalize it to multiphotons, but the output states were distorted [38,39]. It was only recently that better methods were found, which allowed perfect fidelity NLA on states containing up to any chosen number of photons [40–43]. We will show that our proposed scheme can be thought of as a type of generalization to the multiphoton quantum scissor in Ref. [41], in that it can perform teleamplification without photon truncation.

We begin in Sec. II, where we prove that our protocol of size N can in principle perform perfect fidelity NLA of an arbitrary state with N components. We also show our protocol still works with high fidelity in situations where it is misaligned with the input. In Sec. III, we show how our

*joshua.guanzon@uq.net.au

device can also act as a loss-tolerant relay, given we send only coherent states. In Sec. IV, we explore another application for continuous-variable entanglement distillation, which we show is useful even with realistic experimental imperfections. Finally, we conclude in Sec. V.

II. *N*-COMPONENTS CAT TELEAMPLIFIER

Any quantum state can be represented as a superposition of Fock (photon-number) states $|\psi\rangle = \sum_{n=0}^{\infty} c_n|n\rangle$, because these Fock states form a complete basis. Similarly, it is known that any quantum state can be represented as a continuous superposition of coherent states on a circle in phase space because these coherent states also form a complete basis [35]. In this regard, consider

$$|\psi_{N,\alpha}\rangle \equiv \sum_{a=1}^{N} c_a \left|\omega_N^a \alpha\right\rangle, \quad \omega_N \equiv e^{-i2\pi/N}, \tag{1}$$

which is an arbitrarily weighted c_a superposition of N coherent-state components $|\omega_N^a\alpha\rangle$. These coherent states have the same magnitude $|\alpha|$, however, the ath coherent state is rotated by an angle of $-2\pi a/N$. This is shown schematically for $N = 3$ by the three smaller red circles in Fig. 1(a), which lie equally spaced on the perimeter of a larger red circle of radius $|\alpha|$. These states generalize the well-known cat state, therefore, we will name this representation the cat basis.

The NLA operation $g^{a^\dagger a}|\psi_{N,\alpha}\rangle \propto |\psi_{N,g\alpha}\rangle$, with gain $g \in [0, \infty)$, is shown by dashed yellow lines in Fig. 1(a). This transforms the red circle of radius $|\alpha|$ into the blue circle of radius $|g\alpha|$, while preserving all other properties. Our proposed protocol, with a scalable size parameter N, is given schematically in Fig. 1(b) in yellow. In this section, we will prove that this protocol can perform perfect fidelity NLA given the input state can be written as Eq. (1). Hence, as an immediate corollary, our proposed protocol can in principle perform perfect fidelity NLA on any arbitrary input in the asymptotic limit of large N [35]. Note we will show in a later section that even input states which cannot be fully written as Eq. (1) can still experience good quality NLA using our protocol with finite-N sizes.

Our protocol is powered by a resource of light called an N-components cat state

$$|\phi_{N,\beta}\rangle \equiv \frac{1}{\sqrt{\mathcal{N}}} \sum_{b=1}^{N} \omega_N^b \left|\omega_N^b \beta\right\rangle, \tag{2}$$

where $\mathcal{N}$ is the normalization constant. Cat states have been well studied, so there are many techniques to create these states [44–47]; the $N \in \{3, 4\}$ sizes were first made experimentally a decade ago [48,49]. Due to this resource and the basis in which our scheme works, we will call our device the N-components cat teleamplifier (N-CT).

Our device also requires standard linear optical components. We need a beam splitter $B_2(\tau)$ with transmissivity $\tau \in [0, 1]$, which scatters photons between two modes in a linear fashion as $a_1^\dagger \to \sqrt{\tau}a_1^\dagger - \sqrt{1-\tau}a_2^\dagger$. Note $a_m^\dagger$ is the creation operator which acts on the mth mode or port. We also need a balanced N splitter S_N, which similarly has a linear action as $(a_1^\dagger, \ldots, a_N^\dagger)^T \to S_N(a_1^\dagger, \ldots, a_N^\dagger)^T$, with a scattering

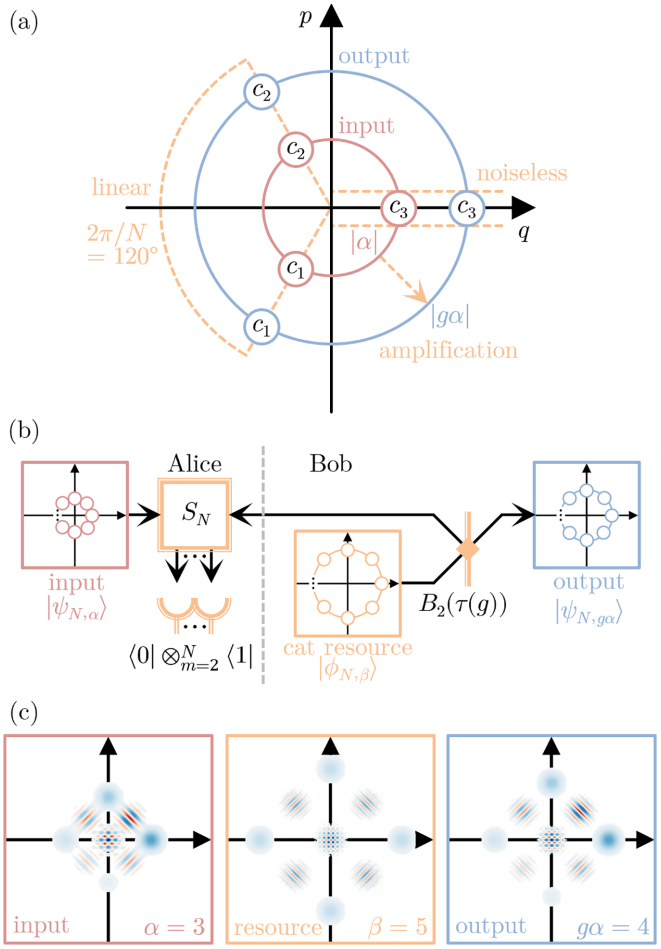

FIG. 1. Any arbitrary quantum state can be described by a continuous superposition of coherent states which lie on a phase-space circle since they form a complete basis [35]. (a) We consider states made from finite-N coherent-state components (here $N = 3$), in a superposition with arbitrary c_a coefficients $|\psi_{N,\alpha}\rangle \equiv \sum_{a=1}^{N} c_a|\omega_N^a\alpha\rangle$, with phase-shift angles $\omega_N \equiv e^{-i2\pi/N}$. An amplification (or deamplification) process changes the circle radius from $|\alpha|$ to $|g\alpha|$ with $g \in [0, \infty)$ gain. (b) Our N-CT proposal performs noiseless linear amplification for any $N \in \mathbb{N}_{\geqslant 2}$, with in principle perfect fidelity. Here Bob starts with an N-component cat state resource with amplitude $\beta = \alpha\sqrt{1+g^2}$, which is split on an unbalanced beam splitter $B_2(\tau)$ with transmissivity $\tau = g^2/(1+g^2)$. Alice then mixes part of Bob's resource with the input state $|\psi_{N,\alpha}\rangle$ on a balanced N splitter S_N. If Alice finds single photons on all N output ports except for the first port $\langle 0| \otimes_{m=2}^{N} \langle 1|$, then this heralds that Bob has an amplified version of the input state $|\psi_{N,g\alpha}\rangle$. (c) Phase-space plots for $N = 4$ coherent states given by blue blobs, with red striped interference fringes due to their superposition with coefficients $\mathbf{c} = [1, 1.5, 2, 2.5]$.

matrix $(S_N)_{j,k} \equiv \omega_N^{(j-1)(k-1)}/\sqrt{N}$. Stated simply, a balanced N splitter is just an N-modes generalization of a balanced beam splitter $S_{N=2} = B_2(\tau = \frac{1}{2})$, with a particular phase configuration defined by the quantum Fourier transformation. Note that these linear transformations can be applied to coherent states by recalling the displacement operator definition $|\alpha\rangle \equiv e^{\alpha a^\dagger - \alpha^* a}|0\rangle$.

We will now explain how our teleamplifier works in an ideal scenario. Bob uses the beam splitter $B_2(\tau)$ to prepare

the following state:

$$B_2(\tau)|0\rangle|\phi_{N,\beta}\rangle = \frac{1}{\sqrt{\mathcal{N}}}\sum_{b=1}^{N}\omega_N^b\big|-\omega_N^b\beta\sqrt{1-\tau}\big\rangle\big|\omega_N^b\beta\sqrt{\tau}\big\rangle$$
$$= \frac{1}{\sqrt{\mathcal{N}}}\sum_{b=1}^{N}\omega_N^b\big|-\omega_N^b\alpha\big\rangle\big|\omega_N^b g\alpha\big\rangle. \quad (3)$$

Bob purposefully chooses a particular amplification gain $g \in [0,\infty)$ by tuning the beam-splitter transmissivity to $\tau = g^2/(1+g^2)$, and preparing the cat resource state with an amplitude of $\beta = \alpha/\sqrt{1-\tau} = \alpha\sqrt{1+g^2}$.

Bob then sends $|-\omega_N^b\alpha\rangle$ towards Alice, who mixes this state on the N splitter S_N with $|\psi_{N,\alpha}\rangle$ resulting in

$$\sum_{a,b=1}^{N}\frac{c_a\omega_N^b}{\sqrt{\mathcal{N}}}\big(S_N\big|\omega_N^a\alpha\big\rangle\big|-\omega_N^b\alpha\big\rangle\otimes_{m=3}^{N}|0\rangle\big)\big|\omega_N^b g\alpha\big\rangle$$
$$= \sum_{a,b=1}^{N}\frac{c_a\omega_N^b}{\sqrt{\mathcal{N}}}\otimes_{m=1}^{N}\big|\big(\omega_N^a-\omega_N^{b+m-1}\big)\alpha/\sqrt{N}\big\rangle\big|\omega_N^b g\alpha\big\rangle. \quad (4)$$

Alice will then perform single-photon measurements on the $m \in \{1,\ldots,N\}$ output ports of the N splitter. Notice that the $m_0 = a-b+1$ output port is guaranteed to have no light since $|(\omega_N^a-\omega_N^{b+m_0-1})\alpha/\sqrt{N}\rangle = |0\rangle$. Put simply, the $b=a$ terms must measure no photons in the first mode $m_0=1$, while the $b\neq a$ terms must measure no photons in a different mode $m_0\neq 1$. Alice exploits this fact by selecting on the measurement outcome $\langle 0|\otimes_{m=2}^{N}\langle 1|$, in which only the $b=a$ terms have nonzero overlap, as follows:

$$\langle 0|\otimes_{m=2}^{N}\langle 1|\ \otimes_{m=1}^{N}\big|\big(\omega_N^a-\omega_N^{b+m-1}\big)\alpha/\sqrt{N}\big\rangle$$
$$= \delta_{b,a}\omega_N^{a(N-1)}\frac{e^{-|\alpha|^2}\alpha^{N-1}}{N^{(N-3)/2}}, \quad (5)$$

where the magnitude is proven in Appendix A.

The unnormalized output state after Alice measures $\langle 0|\otimes_{m=2}^{N}\langle 1|$ will then be

$$|\psi_{N,g\alpha}\rangle = \frac{e^{-|\alpha|^2}\alpha^{N-1}}{N^{(N-3)/2}\sqrt{\mathcal{N}}}\sum_{a=1}^{N}c_a\big|\omega_N^a g\alpha\big\rangle. \quad (6)$$

Therefore, we have proven that our N-CT performs the required NLA operator $g^{a^\dagger a}$ with perfect fidelity, on a superposition of coherent states. In Fig. 1(c), we have plotted an example for $N=4$ of the input, resource, and output superposition states in phase space. We have set the input state coefficients $\mathbf{c}\equiv[c_1,\ldots,c_N]$ such that each component clearly has a different weighting; in our example, we normalize the state based on $\mathbf{c}=[1,1.5,2,2.5]$ as relative weightings. We can see that our technique uses an equally weighted cat resource, to teleport the properties of the input state to the output state with a chosen amplification gain g.

This operation occurs with a success probability given by

$$\mathbb{P} = \langle\psi_{N,g\alpha}|\psi_{N,g\alpha}\rangle. \quad (7)$$

This success probability can be improved by a factor of N, if Alice can select on any measurement of the form $\otimes_{m=1}^{m_0-1}\langle 1|\otimes\langle 0|\otimes_{m=m_0+1}^{N}\langle 1|$, where $m_0\in\{1,\ldots,N\}$ is the mode that measured vacuum. Due to the symmetry of the balanced N splitter, these measurements produce the same output states, but rotated by an angle of $2\pi(m_0-1)/N$. Therefore, this can be physically corrected via a feed-forward mechanism which applies a $\omega_N^{(m_0-1)a^\dagger a}$ phase shift. Alternatively, this can be virtually corrected if Bob is just going to measure the output state, by applying the required rotation on the results via software. A detailed analysis about these N acceptable measurements which can be shown to produce the same output states is given in Appendix B.

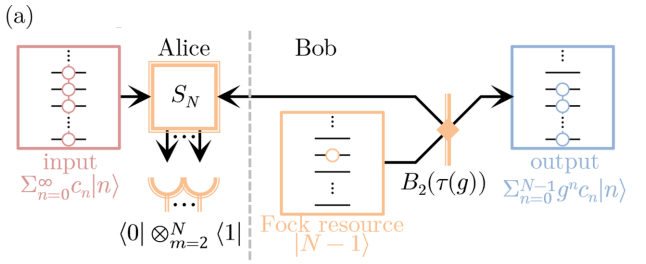

(b)

NLA teleamplifier	Finite N	Asymptotic N
N-FT ($N-1$ quantum scissor)	$\Sigma_{n=0}^{N-1}c_n\|n\rangle$ (N-components Fock)	any state
N-CT (our proposal)	$\Sigma_{n=1}^{N}c_n\|\omega_N^n\alpha\rangle$ (N-components cat)	any state

FIG. 2. (a) Our proposed N-CT protocol is a generalization of the N-FT, or more commonly known as the $(N-1)$-photons quantum scissor [41]. The only difference is that an $|N-1\rangle$ bunched photon state is used as the resource, instead of a $|\phi_{N,\beta}\rangle$ cat state; in fact, in the small amplitude $\beta\to 0$ limit, these two resource states are the same. (b) These two teleamplifiers can NLA N components in their particular basis with perfect fidelity. For asymptotically large N these are complete bases, therefore, in principle perfect fidelity NLA can be done for any quantum state.

The structure of our N-CT device is similar to the $(N-1)$-photons quantum scissor protocol in Ref. [41], shown schematically in Fig. 2. This protocol is an N-components Fock teleamplifier (N-FT) [41], in that it can perform NLA with perfect fidelity on any quantum state which can be written in the form $\sum_{n=0}^{N-1}c_n|n\rangle$. The only difference is that the N-FT is powered by a Fock state $|N-1\rangle$ as a resource of light. In fact, Ref. [50] and Appendix C shows that for low β amplitudes the cat state resource used in N-CT becomes the Fock state resource used in N-FT, where $\lim_{\beta\to 0}|\phi_{N,\beta}\rangle = |N-1\rangle$. In this way, one may consider our N-CT as a type of generalization of the N-FT in Ref. [41]. This resource generalization allows our N-CT device the ability to amplify states without any Fock state truncation, a useful property to have if we want to preserve high-photon correlations. If we assume a fixed amount of resource light β, the success probability of our N-CT scales with respect to gain as $\mathbb{P}\propto|\alpha|^{2(N-1)}\propto(1+g^2)^{-(N-1)}$. This is the same as the N-FT [41] and asymptotically equivalent to the theoretical maximum scaling [36], therefore, we pay no significant success probability price for this generalization. In fact, if we can modify the amount of resource light β, our N-CT can still have significant success probability in the limit of large gain g (a feat which is not

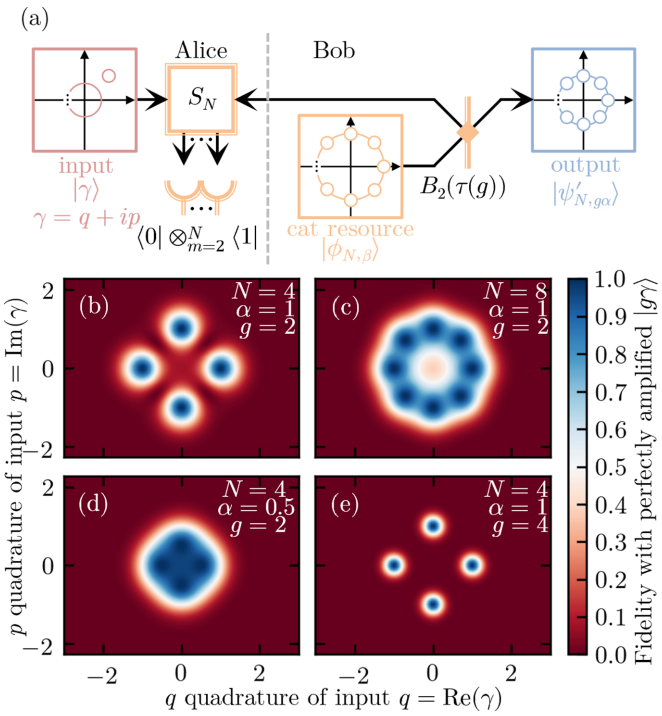

FIG. 3. Suppose we use our N-CT to amplify an arbitrary coherent-state input $|\gamma\rangle$ as in (a), and consider the fidelity against the related perfectly amplified state $|g\gamma\rangle$. We can see in (b) that it does not have to be exactly at the ideal place to be amplified with high fidelity. If we increase the protocol's size parameter N as in (c), then it becomes more phase insensitive. This also happens if we reduce the protocol's expected amplitude parameter α as in (d), but at the cost of being less able to amplify larger states. Finally, if we demand more amplification gain g as in (e), we require more knowledge about the input state to perform this with high fidelity.

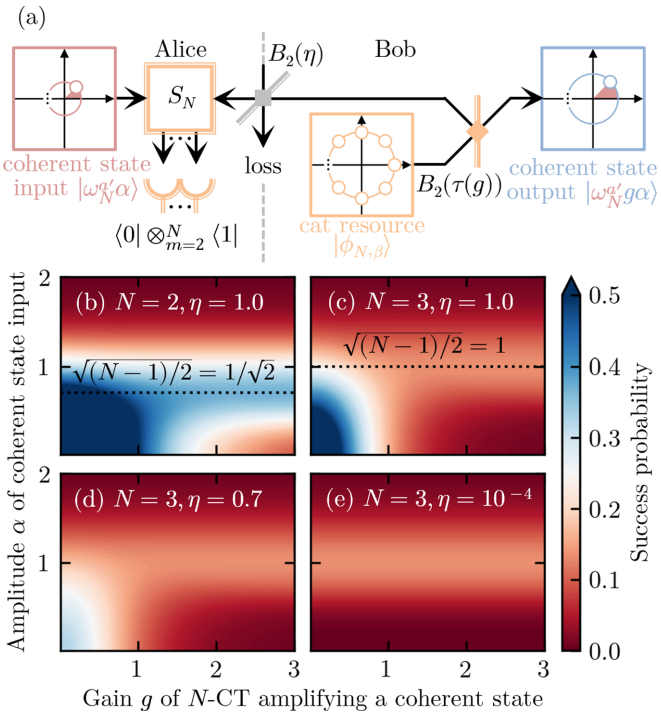

FIG. 4. (a) Alice may choose to send only one coherent state $|\omega_N^{a'}\alpha\rangle$, out of the N possible phase angles $a' \in \{1, \ldots, N\}$. This can be done despite limited transmissivity $\eta \in [0, 1]$ of the channel connecting Alice and Bob (i.e., loss tolerance). Bob needs to take into account of this loss by using a larger cat resource state $\beta = \alpha\sqrt{1/\eta + g^2}$ and setting the beam-splitter $B_2(\tau)$ transmissivity to $\tau = \eta g^2/(1 + \eta g^2)$. As demonstrated in (b) and (c), our N-CT can have good success probability even with asymptotically large gain $g \to \infty$; an input state with $\alpha_{\max} = \sqrt{(N-1)/2}$ amplitude maximizes the success probability. As shown in (c), (d), and (e), loss has minimal effect on probability if we are considering amplification $g > 1$; this holds true even with asymptotically large loss $\eta \to 0$.

possible for the N-FT), which we will show later in the next section.

Let us consider what would happen if the input state $|\gamma\rangle$ is not exactly one of the chosen few coherent states (or any superposition of them), as shown in Fig. 3(a). In Appendix D we prove that the output is still just an N-components coherent-state superposition $|\psi'_{N,g\alpha}\rangle$, whose coefficients depend on the input parameter γ. We also derive an analytical expression for fidelity $F_\gamma \propto |\langle g\gamma|\psi'_{N,g\alpha}\rangle|^2$, which is a comparison with the output state from a perfect NLA $|g\gamma\rangle \propto g^{a^\dagger a}|\gamma\rangle$. This fidelity F_γ is plotted in Figs. 3(b) to 3(e), which show that our device can still amplify with high fidelity even if the input state is misaligned. All quantities plotted in this paper are dimensionless, where we chose the convention $\hbar = \frac{1}{2}$ natural units such that a displacement of α corresponds to the same magnitude in phase space. Our protocol has the physical parameter set $\{N, \beta, \tau\}$, but for ease of understanding we can change this into a more pedagogical parameter set $\{N, \alpha, g\}$. We can interpret $|\alpha|$ as the protocol's expected input magnitude which is the large red circle in Fig. 3(a), while $|g\alpha|$ is the protocol's expected output magnitude which is the large blue circle. The actual input magnitude $|\gamma|$ amplifies well if it is near what is expected $|\alpha|$, as shown in Figs. 3(b) and 3(d). Interestingly, if we increase the gain g this decreases the size of acceptable values, as shown when comparing Figs. 3(b) and 3(e). This makes sense, as any misalignment between the input and protocol will become more apparent at higher gain. In general, if we increase how crowded the coherent states are on the phase-space circle, we increase the phase-space insensitivity of our protocol.

III. LOSS-TOLERANT RELAY OF COHERENT STATES

Suppose that Alice and Bob are now connected by a lossy fiber channel, with a transmissivity of $\eta \in [0, 1]$, as shown in Fig. 4. Loss can be described as another beam splitter $B_2(\eta)$ attached to an extra environment mode. This results in the following shared state:

$$B_2(\eta)B_2(\tau)|0\rangle|\phi_{N,\beta}\rangle|0\rangle = \frac{1}{\sqrt{\mathcal{N}}}\sum_{b=1}^{N} \omega_N^b\big|-\omega_N^b\alpha\big\rangle\big|\omega_N^b g\alpha\big\rangle\big|\omega_N^b\epsilon\big\rangle, \tag{8}$$

where $|\omega_N^b\epsilon\rangle$ describes the light lost to the environment. In contrast to the lossless scenario in Eq. (3), Bob must take the amount of loss into account to achieve a particular gain $g = \sqrt{\tau}/\sqrt{(1-\tau)\eta}$, which means setting his beam-splitter

transmissivity to $\tau = \eta g^2/(1+\eta g^2)$. The amplitude of the cat state resource must also be larger to compensate for the loss $\beta = \alpha/\sqrt{(1-\tau)\eta} = \alpha\sqrt{1+\eta g^2}/\sqrt{\eta}$. Note that the environment mode has an amplitude of $\epsilon = \beta\sqrt{(1-\tau)(1-\eta)} = \alpha\sqrt{1-\eta}/\sqrt{\eta}$, however, it is more important to notice that this error state is correlated in phase ω_N^b.

Now, consider Alice mixing $|-\omega_N^b\alpha\rangle$ with her state $|\psi_{N,\alpha}\rangle$ on the balanced N splitter S_N, and performing N single-photon measurements $\otimes_{m=1}^{m_0-1}\langle 1|\otimes\langle 0|\otimes_{m=m_0+1}^{N}\langle 1|$. Notice that since Eq. (8) is similar to Eq. (3) but with an extra error mode, the output state is similar to Eq. (6) as follows:

$$\frac{e^{-|\alpha|^2}\alpha^{N-1}}{N^{(N-3)/2}\sqrt{\mathcal{N}}}\sum_{a=1}^{N} c_a\left|\omega_N^a g\alpha\right\rangle\left|\omega_N^a\epsilon\right\rangle. \tag{9}$$

This output state is unfortunately entangled with the environment mode. Therefore, if Alice chooses to send any entangled state of the form in Eq. (1), the output Bob receives will have decoherence type errors (in which cat states are particularly vulnerable). Since detector inefficiencies can be modeled as loss, Eq. (9) also suggests our amplifier can be susceptible to experimental imperfections, depending on the input state. This is explored in Appendix E, where we show amplified superposition states will have suppressed interference fringes due to inefficient detectors. One exception is for the low-amplitude case since our N-CT protocol reduces down to the N-FT quantum scissor protocol, which is already known to be tolerant against experimental imperfections [40,41].

Our device is also tolerant to loss effects in the case where Alice instead chooses to send just one coherent state $|\omega_N^{a'}g\alpha\rangle$ (i.e. $c_a = \delta_{a,a'}$). This is because the output state given in Eq. (9) will be

$$\left|\omega_N^{a'}g\alpha\right\rangle\left|\omega_N^{a'}\epsilon\right\rangle, \tag{10}$$

which is separable from the environment (note this is also the case if Alice sends a mixture of coherent states). In other words, Alice can send information to Bob in a loss-tolerant manner, by encoding information via the phase shift of coherent states $a' \in \{1,\ldots,N\}$. Note that with $N=2$, only binary information can be sent. Our fully scalable N-CT protocol means this can now be done with any number of phases N, which means N-ary information can now be sent in a loss-tolerant manner.

This protocol is not only loss tolerant in terms of output state fidelity, but also success probability. If we substitute in $c_a = \delta_{a,a'}$ into the unnormalized output state in Eq. (9), we can get the following success probability:

$$\mathbb{P}_c = \frac{e^{-2|\alpha|^2}|\alpha|^{2(N-1)}}{N^{(N-3)}\mathcal{N}}, \tag{11}$$

$$\mathcal{N} = \sum_{j,k=1}^{N}\omega_N^{k-j}e^{(\omega_N^{k-j}-1)|\alpha|^2(1/\eta+g^2)}. \tag{12}$$

We have plotted $N\mathbb{P}_c$ as contour graphs in Fig. 4 for particular values of $\{N,\alpha,g,\eta\}$, which shows that even large gain and/or large loss can still have good success probability. This holds true even asymptotically with $g\to\infty$ and $\eta\to 0$ because physically the resource light is increased $\beta = \alpha\sqrt{1/\eta+g^2}$ to achieve the necessary gain and compensate for any loss (hence $\mathcal{N}\to N$ in these limits). In contrast, the N-FT uses a fixed resource state which means its success probability will always scale as $(1+g^2)^{-(N-1)}$ [41]. Hence, our proposed resource generalization via the N-CT results in a significant success probability advantage. Note that the maximum success probability in these asymptotic limits is $\frac{2eN^2}{N-1}(\frac{N-1}{2eN})^N$, which occurs with $\alpha_{\max} = \sqrt{(N-1)/2}$ amplitude inputs. More detailed analysis on the success probability can be found in Appendix F.

Recall that this protocol increases the coherent-state magnitude without changing the uncertainty profile, therefore, this has applications towards discriminating between various overlapping nonorthogonal states [51,52]. Our teleamplifier could also be useful for QKD purposes via multiarrayed phase-shift keyed (N-PSK) coherent states. For example, the B92 protocol [53] could be done using 2-PSK coherent states [54,55], while the BB84 protocol [56] could be done using 4-PSK coherent states [32,57]. One may consider the in-between 3-PSK coherent-states case, which is secure for CV QKD [58]. Finally, it is known for arbitrary N-PSK coherent states, with CV QKD and reverse reconciliation, that increasing N improves the secret key rate [59]. However, whether these security proofs and rate details hold with a postselected amplifier is unknown, hence, we will leave QKD applications as an open question for future research.

Lastly, note that coherent states put through a pure loss channel cause a decrease in amplitude without any change in noise profile or phase angle. Hence,it is possible to put another loss channel between the input and the S_N component in Fig. 4, without changing the output (aside from a reduction in amplitude). This means if we want to transfer these coherent states over a particular length of optical fiber, then it is a good idea to put S_N in the middle of the fiber, as this would mean the loss before and after S_N is balanced. This setup is extremely useful for quantum relay purposes. In fact, the $N=1$ CT can overcome the repeaterless bound [60], which sets the benchmark for quantum repeaters, without requiring quantum memories [61,62].

IV. CONTINUOUS-VARIABLE ENTANGLEMENT DISTILLATION

Quantum entanglement is a useful resource for many protocols. However, maintaining this entanglement from environmental loss and other imperfections is a major challenge. To make this more concrete, consider a scenario where Alice has a two-mode squeezed vacuum (TMSV) state $|\chi\rangle = \sqrt{1-\chi^2}\sum_{k=0}^{\infty}\chi^k|k\rangle|k\rangle$, where $\chi\in[0,1)$ is the squeezing parameter. A particular measure of continuous-variable entanglement is the Gaussian entanglement of formation E [63–65], which can be calculated numerically using the quantum state's covariance matrix [66,67]. If Alice's TMSV state is moderately squeezed by $\chi = 0.25$, then initially the amount of entanglement between the two modes of this state is $E(\chi=0.25,\eta=1)\approx 0.36$. However, suppose Alice sends one mode of the TMSV state through a channel to Bob, but unfortunately this channel only has a transmissivity of $\eta = 0.05$ (meaning that any light put through it will experience

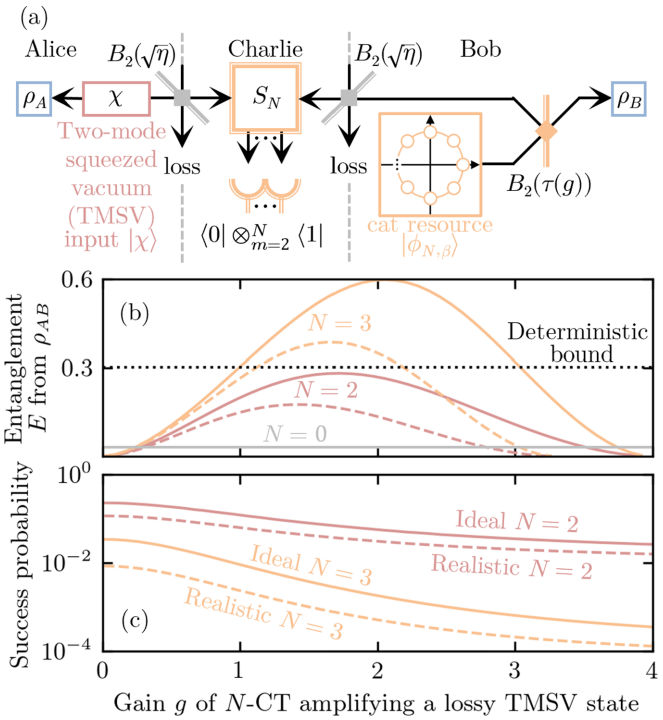

FIG. 5. Suppose Alice wants to share a high-quality entangled state with Bob, however, they are connected by an imperfect channel which causes 95% loss (i.e., $\eta = 0.05$ transmissivity). If Alice sends one arm of a moderately squeezed TMSV state $|\chi = 0.25\rangle$ to Bob, the resultant entanglement E will be limited as shown by the solid gray $N = 0$ line in (b). Note this entanglement is the Gaussian entanglement of formation E. Even if Alice starts with an maximally squeezed TMSV state $|\chi \to 1\rangle$, the loss will still greatly limit the amount of entanglement, as shown by the dotted black line; this is called the deterministic bound. Our proposed N-CT in (a) can be used for probabilistic entanglement distillation. This recovers entanglement above the deterministic bound, depending on the size of our protocol N as shown in (b). This holds even if we consider realistic experimental imperfections on the detectors and cat resource, as shown by the dashed lines. However, this additional entanglement comes at a cost in that the N-CT is probabilistic, with a success probability shown in (c).

95% loss). This resultant lossy TMSV state ρ_{AB} now only has $E(\chi = 0.25, \eta = 0.05) \approx 0.03$ entanglement, as indicated by the $N = 0$ labeled solid gray line in Fig. 5(b). Even if Alice starts off with an maximally squeezed state $\chi \to 1$ which approaches infinite entanglement, this loss limits the entanglement to only $E(\chi \to 1, \eta = 0.05) \approx 0.30$, as indicated by the horizontal dotted black line. This quantity is called the deterministic bound, as it is the best you can do without a probabilistic entanglement recovery process.

Our N-CT device can be used to probabilistically distill entanglement through a lossy channel, as shown schematically in Fig. 5(a). We have positioned the N splitter S_N in the middle of the channel as this greatly improves the success probability scaling to $O(\sqrt{\eta})$. We choose a particular gain g and set Bob's beam-splitter transmissivity to $\tau = g^2/(1 + g^2)$. Note that this lossy TMSV input state cannot be fully written in the finite-N-components cat basis form given in Eq. (1). Therefore, we simply optimize the cat resource amplitude β for each gain g to maximize the amount of entanglement E.

The resultant entanglement distillation for $\chi = 0.25$, using $N = 2$ and 3 sizes is given by the solid red and yellow lines, respectively, in Fig. 5(b). If we include experimental imperfections, modeled by 30% extra loss on the cat state resource and 70% efficiency single-photon detectors [68–71], we get the dashed lines. Even accounting for realistic experimental imperfections, we can see that increasing the size N increases the entanglement. The reason for the bell-shaped curves could be understood by considering how the transmissivity τ of the beam splitter $B_2(\tau)$ changes with gain g. Small gain $g \to 0$ means limited transmissivity $\tau \to 0$, which results in limited amount of light exiting on Bob's side. On the other hand, large gain $g \to \infty$ means almost complete transmissivity $\tau \to 1$, which results in not much of the resource light being entangled with Alice's input. From this physical intuition, there should be an optimal gain g in which the amount of entanglement E is maximized.

This extra entanglement comes at the cost of success probability as shown in Fig. 5(c). However, our generalized N-CT device can beat the deterministic bound by using higher-N values, thus demonstrating its usefulness for generating high-quality entanglement. This also clearly shows that our N-CT device is useful even if the input state does not fully satisfy Eq. (1).

V. CONCLUSION

We have proven that our N-CT protocol, given in Fig. 1(b), can be used to implement the noiseless linear amplification operator $g^{a^\dagger a}$. This can be done with perfect fidelity, if the input state can be fully written in the N-components cat basis as Eq. (1). Since this basis is complete given asymptotic number of components $N \to \infty$, this means the N-CT can in principle perform perfect fidelity amplification on any quantum state. These results can be understood as an extension to the generalized quantum scissor N-FT protocol [41], where the output state has no Fock truncation. We also demonstrated that our N-CT can still work with high fidelity even if the input does not align exactly with Eq. (1). Furthermore, we have shown that if the input is one out of a set of N coherent states, then amplification can be done in a loss-tolerant manner without decoherence, and with a significant success probability even in the large gain and large loss asymptotic limit. Therefore, our proposal also has uses for many quantum protocols which employ N-ary phase-shift keyed coherent states. Finally, we have also shown that our proposed N-CT device for finite N is able to distill high-quality continuous-variable entanglement through lossy channels, even assuming realistic experimental imperfections.

All our simulation code and data are available in Github [72].

ACKNOWLEDGMENTS

A.P.L. acknowledges support from BMBF (QPIC) and the Einstein Research Unit on Quantum Devices. This research was supported by the Australian Research Council Centre of

Excellence for Quantum Computation and Communication Technology (Project No. CE170100012).

APPENDIX A: PROOF OF MEASUREMENT AMPLITUDE

The measurement amplitude resolves to

$$\begin{aligned}
&\langle 0|\otimes_{m=2}^{N}\langle 1|\ \otimes_{m=1}^{N}\left|\left(\omega_N^a-\omega_N^{b+m-1}\right)\alpha/\sqrt{N}\right\rangle\\
&=\delta_{b,a}\langle 0|\otimes_{m=2}^{N}\langle 1|\ \otimes_{m=1}^{N}\left|\left(1-\omega_N^{m-1}\right)\omega_N^a\alpha/\sqrt{N}\right\rangle\\
&=\delta_{b,a}e^{-\sum_{m=2}^{N}|1-\omega_N^{m-1}|^2|\alpha|^2/2N}\prod_{m=2}^{N}\frac{\left(1-\omega_N^{m-1}\right)\omega_N^a\alpha}{\sqrt{N}}\\
&=\delta_{b,a}\omega_N^{a(N-1)}\frac{e^{-|\alpha|^2}\alpha^{N-1}}{N^{(N-1)/2}}\prod_{m=2}^{N}\left(1-\omega_N^{m-1}\right)\\
&=\delta_{b,a}\omega_N^{a(N-1)}\frac{e^{-|\alpha|^2}\alpha^{N-1}}{N^{(N-3)/2}}.
\end{aligned}\tag{A1}$$

We will justify all the critical steps of this derivation. The first equality in Eq. (A1) uses the fact that the state $\otimes_{m=1}^{N}|(\omega_N^a-\omega_N^{b+m-1})\alpha/\sqrt{N}\rangle$ has vacuum in the wrong mode other than $b=a$, as explained in detail in the main text after Eq. (4). The second equality in Eq. (A1) used the representation of coherent states in the Fock basis $|\alpha\rangle=e^{-|\alpha|^2/2}\sum_{n=0}^{\infty}\alpha^n/\sqrt{n!}|n\rangle$.

The third equality in Eq. (A1) uses the following to simplify the exponent:

$$\begin{aligned}
\sum_{m=2}^{N}\left|1-\omega_N^{m-1}\right|^2&=\sum_{m=1}^{N}\left|1-\omega_N^{m-1}\right|^2\\
&=\sum_{m=1}^{N}\left(1-\omega_N^{m-1}\right)\left(1-\omega_N^{-m+1}\right)\\
&=\sum_{m=1}^{N}\left(2-\omega_N^{m-1}-\omega_N^{-m+1}\right)\\
&=2N,
\end{aligned}\tag{A2}$$

where we used the geometric summation equation $\sum_{m=1}^{N}\omega_N^{m-1}=(1-\omega_N^N)/(1-\omega_N)=0$, and similarly for $\sum_{m=1}^{N}\omega_N^{-m+1}$.

The final equality in Eq. (A1) uses

$$\prod_{m=2}^{N}\left(1-\omega_N^{m-1}\right)=\prod_{m=1}^{N-1}\left(1-\omega_N^{m}\right)=N,\tag{A3}$$

which we will derive based on the fact that $\omega_N\equiv e^{-2i\pi/N}$ are roots of unity. Consider the following polynomial:

$$p(z)=z^N-1.\tag{A4}$$

The condition $p(z)=0$ is true when $z=e^{-2i\pi k/N}=\omega_N^k$ for $k\in\{0,\ldots,N-1\}$; in other words, ω_N^k are the unique roots of unity. Therefore, this polynomial can also be written in factorization form using these roots

$$p(z)=\prod_{k=0}^{N-1}\left(z-\omega_N^k\right)=(z-1)\prod_{k=1}^{N-1}\left(z-\omega_N^k\right).\tag{A5}$$

Using some basic algebraic manipulation, this same polynomial can also be written as

$$\begin{aligned}
p(z)&=(z+z^2+\cdots+z^N)-(1+z+\cdots+z^{N-1})\\
&=(z-1)(1+z+\cdots+z^{N-1}).
\end{aligned}\tag{A6}$$

Thus, comparing Eqs. (A5) and (A6) we can see that

$$\prod_{k=1}^{N-1}\left(z-\omega_N^k\right)=1+z+\cdots+z^{N-1}.\tag{A7}$$

By substituting in $z=1$, the right-hand side of this expression is equivalent to N since there are N terms. Thus, we have proven our required relation.

APPENDIX B: ALICE MULTIPLE MEASUREMENTS PROOF

We will prove here that Alice can select on a set of N measurements $\otimes_{m=1}^{m_0-1}\langle 1|\otimes\langle 0|\otimes_{m=m_0+1}^{N}\langle 1|$, and produce the same output state $|g\psi_{N,\alpha}\rangle$ but with a correctable phase shift. Note that m_0 refers to the mode or output port of the balanced N splitter which measured vacuum.

Recall from Eq. (4) that the state Alice and Bob share just after the balanced N splitter is

$$\sum_{a,b=1}^{N}c_a\omega_N^b\otimes_{m=1}^{N}\left|\left(\omega_N^a-\omega_N^{b+m-1}\right)\alpha/\sqrt{N}\right\rangle\left|\omega_N^b g\alpha\right\rangle.\tag{B1}$$

Each term $\otimes_{m=1}^{N}|(\omega_N^a-\omega_N^{b+m-1})\alpha/\sqrt{N}\rangle$ is guaranteed to measure vacuum in one output port $m=m_0$, which is when $\omega_N^a=\omega_N^{b+m_0-1}$ or $m_0=a-b+1$.

Now, let us suppose Alice selects on a measurement where all output ports clicked with one photon, except for one port $m=m_0$. This could only have occurred due to the $b=a-m_0+1$ terms because the $b\neq a-m_0+1$ terms are required to measure vacuum in mode $m\neq m_0$. In other words, all terms in the sum where $b\neq a-m_0+1$ have their vacuum state in the wrong mode to be able to satisfy the one-photon detection measurements. Thus, this measurement results in

$$\begin{aligned}
&\otimes_{m=1}^{m_0-1}\langle 1|\otimes\langle 0|\otimes_{m=m_0+1}^{N}\langle 1|\otimes_{m=1}^{N}\left|\left(\omega_N^a-\omega_N^{b+m-1}\right)\alpha/\sqrt{N}\right\rangle\\
&=\delta_{b,a-m_0+1}e^{-\sum_{m=1}^{N}|1-\omega_N^{m-m_0}|^2|\alpha|^2/(2N)}\\
&\quad\times\prod_{m=1}^{m_0-1}\frac{\left(\omega_N^a-\omega_N^{a+m-m_0}\right)\alpha}{\sqrt{N}}\prod_{m=m_0+1}^{N}\frac{\left(\omega_N^a-\omega_N^{a+m-m_0}\right)\alpha}{\sqrt{N}}\\
&=\delta_{b,a-m_0+1}\omega_N^{a(N-1)}\frac{e^{-|\alpha|^2}\alpha^{N-1}}{N^{(N-1)/2}}\\
&\quad\times\prod_{m=1}^{m_0-1}\left(1-\omega_N^{m-m_0}\right)\prod_{m=m_0+1}^{N}\left(1-\omega_N^{m-m_0}\right)\\
&=\delta_{b,a-m_0+1}\omega_N^{a(N-1)}\frac{e^{-|\alpha|^2}\alpha^{N-1}}{N^{(N-3)/2}}.
\end{aligned}\tag{B2}$$

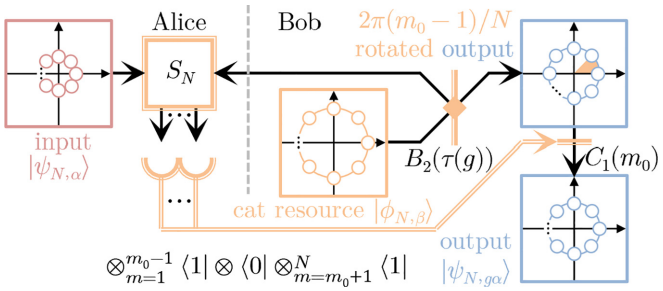

FIG. 6. Alice is free to select on N different measurement outcomes of the form $\otimes_{m=1}^{m_0-1}\langle 1|\otimes\langle 0|\otimes_{m=m_0+1}^{N}\langle 1|$ for $m_0\in\{1,\ldots,N\}$. Note that $m=m_0$ is the output port or mode of the N splitter S_N that measured the vacuum outcome. Due to the symmetry of S_N, these measurements all produce the same output states but phase space rotated by $2\pi(m_0-1)/N$, which can be corrected as explained in text.

The second equality uses $\sum_{m=1}^{N}|1-\omega_N^{m-m_0}|^2=2N$ for the exponent, which can be proven like Eq. (A2). The last equality uses

$$\begin{aligned}
&\prod_{m=1}^{m_0-1}\left(1-\omega_N^{m-m_0}\right)\prod_{m=m_0+1}^{N}\left(1-\omega_N^{m-m_0}\right)\\
&=\prod_{m=-m_0+1}^{-1}\left(1-\omega_N^{m}\right)\prod_{m=1}^{N-m_0}\left(1-\omega_N^{m}\right)\\
&=\prod_{m=N-m_0+1}^{N-1}\left(1-\omega_N^{m}\right)\prod_{m=1}^{N-m_0}\left(1-\omega_N^{m}\right)\\
&=\prod_{m=1}^{N-1}\left(1-\omega_N^{m}\right)\\
&=N,
\end{aligned}\tag{B3}$$

using $\omega_N^N=1$ and Eq. (A3).

Applying the result in Eq. (B2) to (B1) produces the following output state:

$$\begin{aligned}
&\omega_N^{-m_0+1}\frac{e^{-|\alpha|^2}\alpha^{N-1}}{N^{(N-3)/2}\sqrt{\mathcal{N}}}\sum_{a=1}^{N}c_a\left|\omega_N^{a-m_0+1}g\alpha\right\rangle\\
&=\omega_N^{(-m_0+1)(1+a^\dagger a)}|g\psi_{N,\alpha}\rangle.
\end{aligned}\tag{B4}$$

Therefore, we have shown irrespective of m_0, Bob can always recover the same output state by applying a phase-shift correction of

$$C_1(m_0)=\omega_N^{(m_0-1)a^\dagger a},\tag{B5}$$

which we show schematically in Fig. 6. Note this correction does not need to be implemented physically if Bob is simply measuring the output state, rather the required rotation correction can be implemented in software directly on Bob's measurement results. These measurements also have the same probability of success $\mathbb{P}=\langle g\psi_{N,\alpha}|g\psi_{N,\alpha}\rangle$, irrespective of m_0. Therefore, if all N measurements can be accepted, then we can improve the success probability by a factor of N to $N\mathbb{P}$.

APPENDIX C: CAT RESOURCE STATE IN FOCK BASIS

We can represent the cat state resource in the Fock basis as

$$\begin{aligned}
|\phi_{N,\beta}\rangle&\equiv\frac{1}{\sqrt{\mathcal{N}}}\sum_{b=1}^{N}\omega_N^b\left|\omega_N^b\beta\right\rangle\\
&=\frac{e^{-|\beta|^2/2}}{\sqrt{\mathcal{N}}}\sum_{b=1}^{N}\sum_{n=0}^{\infty}\omega_N^{b(n+1)}\frac{\beta^n}{\sqrt{n!}}|n\rangle,
\end{aligned}\tag{C1}$$

where we used the coherent-state representation $|\alpha\rangle=e^{-|\alpha|^2/2}\sum_{n=0}^{\infty}\alpha^n/\sqrt{n!}|n\rangle$. Note that most of these terms resolve to zero since

$$\sum_{b=1}^{N}\omega_N^{b(n+1)}=\delta_{n+1,kN}N,\quad k\in\mathbb{N}.\tag{C2}$$

This is because when $\omega_N^{b(n+1)}\neq 1$ [i.e., $(n+1)\neq kN$], then the expression is the sum of all roots of unity which resolves to zero, or algebraically $\omega_N^{n+1}(1-\omega_N^{N(n+1)})/(1-\omega_N^{n+1})=0$. This means that our resource state can be simplified as

$$|\phi_{N,\beta}\rangle=\frac{Ne^{-|\beta|^2/2}}{\sqrt{\mathcal{N}}}\sum_{k=1}^{\infty}\frac{\beta^{kN-1}}{\sqrt{(kN-1)!}}|kN-1\rangle.\tag{C3}$$

Notice that for very small amplitudes $\beta\ll 1$, the term with the largest coefficient will overwhelmingly be the $k=1$ term. From this, it is clear that for asymptotically small amplitudes this cat state reduces down to $\lim_{\beta\to 0}|\phi_{N,\beta}\rangle=|N-1\rangle$. Note that this result was already known, as detailed in Ref. [50].

APPENDIX D: ARBITRARY COHERENT-STATE INPUT

Here we consider our proposed amplifier given the input is just any arbitrary coherent state (i.e., it is not in one of the fixed places in phase space) as

$$|\gamma\rangle,\quad \gamma=q+ip=re^{i\theta},\tag{D1}$$

assuming ideal conditions.

Recall from Eq. (3) that Bob prepares

$$B_2(\tau)|0\rangle|\phi_{N,\beta}\rangle=\frac{1}{\sqrt{\mathcal{N}}}\sum_{b=1}^{N}\omega_N^b\left|-\omega_N^b\alpha\right\rangle\left|\omega_N^b g\alpha\right\rangle.\tag{D2}$$

Note here α is now the *expected* input amplitude that we set by choosing the cat resource amplitude β. Bob then sends $|-\omega_N^b\alpha\rangle$ towards Alice, who mixes this state on the N splitter S_N with $|\gamma\rangle$ resulting in

$$\begin{aligned}
&\sum_{b=1}^{N}\frac{\omega_N^b}{\sqrt{\mathcal{N}}}\left(S_N|\gamma\rangle\left|-\omega_N^b\alpha\right\rangle\otimes_{m=3}^{N}|0\rangle\right)\left|\omega_N^b g\alpha\right\rangle\\
&=\sum_{b=1}^{N}\frac{\omega_N^b}{\sqrt{\mathcal{N}}}\otimes_{m=1}^{N}\left|\left(\gamma-\omega_N^{b+m-1}\alpha\right)/\sqrt{N}\right\rangle\left|\omega_N^b g\alpha\right\rangle.
\end{aligned}\tag{D3}$$

Alice will herald on the single-photon measurements $\langle 0|\otimes_{m=2}^{N}\langle 1|$, which requires the amplitude

$$\begin{aligned}
&\langle 0|\otimes_{m=2}^{N}\langle 1|\ \otimes_{m=1}^{N}\left|\left(\gamma-\omega_N^{b+m-1}\alpha\right)/\sqrt{N}\right\rangle \\
&\quad= e^{-\sum_{m=1}^{N}|\gamma-\omega_N^{b+m-1}\alpha|^2/(2N)}\prod_{m=2}^{N}\frac{\gamma-\omega_N^{b+m-1}\alpha}{\sqrt{N}} \\
&\quad= \frac{e^{-(|\gamma|^2+|\alpha|^2)/2}}{N^{(N-1)/2}}\prod_{m=2}^{N}\left(\gamma-\omega_N^{b+m-1}\alpha\right) \\
&\quad= \frac{e^{-(|\gamma|^2+|\alpha|^2)/2}}{N^{(N-1)/2}}d_b. \qquad \text{(D4)}
\end{aligned}$$

We simplified the exponent as

$$\begin{aligned}
&\sum_{m=1}^{N}\left|\gamma-\omega_N^{b+m-1}\alpha\right|^2 \\
&\quad=\sum_{m=1}^{N}\left(|\gamma|^2+|\alpha|^2-\omega_N^{b+m-1}\gamma^*\alpha-\omega_N^{-b-m+1}\gamma\alpha^*\right) \\
&\quad= N(|\gamma|^2+|\alpha|^2), \qquad \text{(D5)}
\end{aligned}$$

where we used $\sum_{m=1}^{N}\omega_N^{m-1}=(1-\omega_N^N)/(1-\omega_N)=0$. We also simplified the product as follows:

$$\begin{aligned}
d_b &= \prod_{m=2}^{N}\left(\gamma-\omega_N^{b+m-1}\alpha\right) \\
&= \prod_{m=1}^{N-1}\left(\gamma-\omega_N^{b+m}\alpha\right) \\
&= \omega_N^{b(N-1)}\alpha^{N-1}\prod_{m=1}^{N-1}\left(\frac{\gamma}{\omega_N^b\alpha}-\omega_N^m\right) \\
&= \omega_N^{b(N-1)}\alpha^{N-1}\sum_{m=1}^{N}\left(\frac{\gamma}{\omega_N^b\alpha}\right)^{m-1} \\
&= \omega_N^{b(N-1)}\alpha^{N-1}\frac{1-\gamma^N/\left(\omega_N^b\alpha\right)^N}{1-\gamma/\left(\omega_N^b\alpha\right)} \\
&= \frac{\left(\omega_N^b\alpha\right)^N-\gamma^N}{\omega_N^b\alpha-\gamma}, \qquad \text{(D6)}
\end{aligned}$$

where we used Eq. (A7) in the fourth equality, and assumed that $\gamma\neq\omega_N^b\alpha$ to resolve the geometric sum in the fifth equality. If $\gamma=\omega_N^b\alpha$, then $d_b=\omega_N^{b(N-1)}\alpha^{N-1}N$ which when substituted in Eq. (D4) we get an expression which is consistent with our previous Eq. (A1) result.

By using the derived amplitude in Eq. (D4), we can see that applying these single-photon measurements to Eq. (D3) produces the unnormalized output state

$$|\psi'_{N,g\alpha}\rangle=\frac{e^{-(|\gamma|^2+|\alpha|^2)/2}}{N^{(N-1)/2}\sqrt{\mathcal{N}}}\sum_{b=1}^{N}\omega_N^b d_b\left|\omega_N^b g\alpha\right\rangle. \qquad \text{(D7)}$$

We may then calculate the success probability of this protocol as

$$\begin{aligned}
\mathbb{P}_\gamma &= \langle\psi'_{N,g\alpha}|\psi'_{N,g\alpha}\rangle \\
&= \frac{e^{-|\gamma|^2-|\alpha|^2}}{N^{(N-1)}\mathcal{N}}\sum_{a,b=1}^{N}\omega_N^{b-a}d_b d_a^*\langle\omega_N^a g\alpha|\omega_N^b g\alpha\rangle \\
&= \frac{e^{-|\gamma|^2-|\alpha|^2-|g\alpha|^2}}{N^{(N-1)}\mathcal{N}}\sum_{a,b=1}^{N}\omega_N^{b-a}d_b d_a^* e^{\omega_N^{b-a}|g\alpha|^2}. \qquad \text{(D8)}
\end{aligned}$$

We can then calculate the fidelity of this protocol as

$$\begin{aligned}
F_\gamma &= \frac{1}{\mathbb{P}_\gamma}|\langle g\gamma|\psi'_{N,g\alpha}\rangle|^2 \\
&= \frac{1}{\mathbb{P}_\gamma}\left|\frac{e^{-(|\gamma|^2+|\alpha|^2)/2}}{N^{(N-1)/2}\sqrt{\mathcal{N}}}\sum_{b=1}^{N}\omega_N^b d_b\langle g\gamma|\omega_N^b g\alpha\rangle\right|^2 \\
&= \frac{1}{\mathbb{P}_\gamma}\frac{e^{-|\gamma|^2-|\alpha|^2-|g\gamma|^2-|g\alpha|^2}}{N^{(N-1)}\mathcal{N}}\left|\sum_{b=1}^{N}\omega_N^b d_b e^{\omega_N^b g^2\gamma^*\alpha}\right|^2 \\
&= \frac{e^{-|g\gamma|^2}\left|\sum_{b=1}^{N}\omega_N^b d_b e^{\omega_N^b g^2\gamma^*\alpha}\right|^2}{\sum_{a,b=1}^{N}\omega_N^{b-a}d_b d_a^* e^{\omega_N^{b-a}|g\alpha|^2}}. \qquad \text{(D9)}
\end{aligned}$$

We plot these formulas in Figs. 3 and 7 for fidelity, and in Fig. 8 for success probability. This is done for various parameter settings of our protocol, including the amount of coherent-state components N, the expected amplitude α, and the amplitude gain g.

Note that, in general, fidelity is not always a good figure of merit since two states that share a high fidelity could still have significantly different physical properties [73–76]. In our case we are comparing two pure states, such that fidelity is the overlap between the states squared. Furthermore, we have points in Figs. 3 and 7 where the fidelity is unity $F_\gamma=1$. In this regard, these graphs just give a qualitative indication for what input coherent states are most appropriate for a given amplifier parameter set, and how changing these parameters can affect the outcome. Due to the limitations of fidelity, another figure of merit should be used depending on the application under consideration for the amplifier; as an example, in Sec. IV we used entanglement of formation as a measure for entanglement distillation.

APPENDIX E: EXPERIMENTAL IMPERFECTION ANALYSIS

The effect of experimental imperfections is an important consideration for any suggested experimental device. In a quantum optical device such as our teleamplifier, one major consideration will be detector inefficiencies and loss. Note that a 70% efficient detector can be modeling by a beam splitter with 70% transmissivity (in other words, a 30% loss channel) in front of an idealized 100% efficient detector. The effect of this imperfection for our proposed teleamplifier is demonstrated by the Wigner functions in Fig. 9. In the upper row, we consider amplifying a small-amplitude cat state given in Fig. 9(a) using the 2-CT device. We can see by contrasting the inefficient detector case in Fig. 9(b) with the ideal in

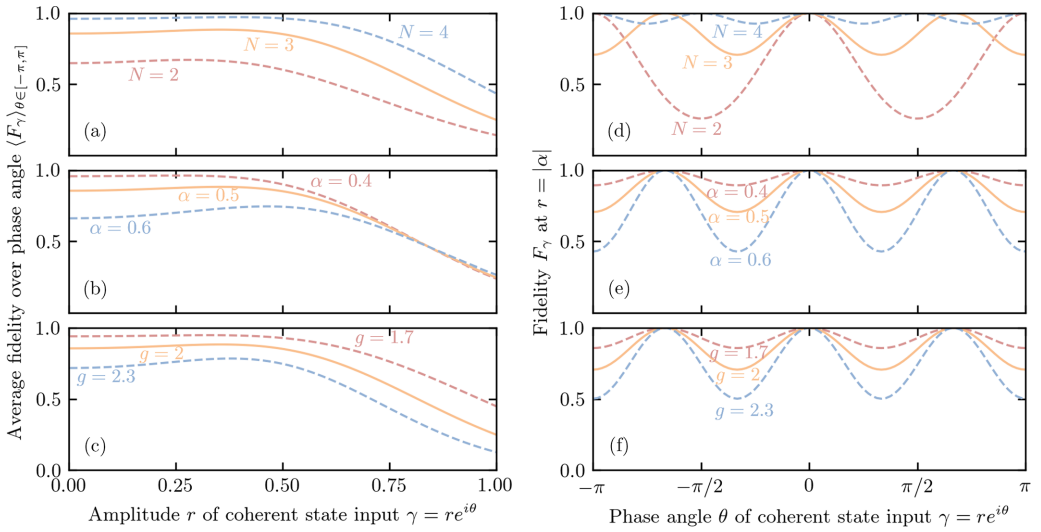

FIG. 7. Here we use fidelity F_γ as a measure for how well our device can amplify a completely arbitrary coherent state $|\gamma\rangle$ to $|g\gamma\rangle$. The left graphs, (a)–(c), are the fidelity for amplifying a coherent state with $r = |\gamma|$ amplitude, averaged equally over all phase angles $\theta = \arg(\gamma) \in [-\pi, \pi]$. The right graphs, (d)–(f), are the fidelity for amplifying a coherent state with θ phase angle, with a fixed amplitude of $r = |\alpha|$. The solid orange lines were calculated using the chosen default parameter setting of $\{N = 3, \alpha = 0.5, g = 2\}$, which can be compared to the dashed lines where one parameter of this set is changed. We can see in (a) and (d) that as the number of components N increases, the fidelity increases because more phase angles can be amplified well (i.e., it becomes more linear due to overlapping components). From (b) and (e), we can see as the expected amplitude α becomes smaller, the protocol becomes more linear. Finally, (c) and (f) show that as we demand more amplification gain g, we require more specific knowledge about the input state γ to amplify with good fidelity.

Fig. 9(c) that the effect of this experimental imperfection is the suppression of the fringes. This is not surprising considering the well-known vulnerability of cat states to decoherence effects via loss. However, clearly this effect is not relevant if we consider just amplifying a single coherent state such as in Fig. 9(d). In this case, the 2-CT device will produce an output state using imperfect detectors in Fig. 9(e), which is essentially the same as using ideal detectors in Fig. 9(f).

Another potential source of experimental imperfection is misalignment between the input state and the resource state for a given N-CT. This was explored in Appendix D for the case of a single coherent-state input, which showed some good fidelity even with some misalignment. Here we consider the effect of misalignment for coherent-state superposition inputs, as shown in Fig. 10. The expected input state is an unbalanced cat state given in Fig. 10(a), in which a perfectly aligned device produces the amplified state in Fig. 10(b). Now, from Figs. 10(c)–10(f) we apply an increasingly larger rotation to the input state (i.e., phase misalignment) before amplifying using the same device. Similarly, from Figs. 10(g)–10(i) we scale the amplitude of the input state (i.e., amplitude misalignment) before amplifying using the same device. We

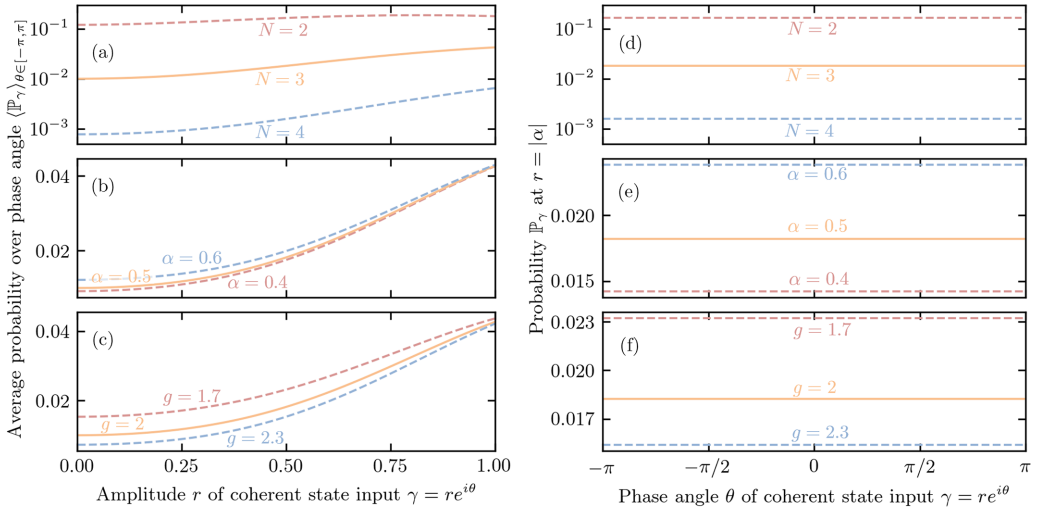

FIG. 8. This is the same setting as Fig. 7, except we are considering the success probability $\mathbb{P}_\gamma$ for amplifying $|\gamma\rangle$. Based on the right graphs, (d)–(f), it is clear that the input phase θ does not affect how likely we will get correct detection events. We can see that the parameter N has the largest effect on the success probability, while α and g have limited impact.

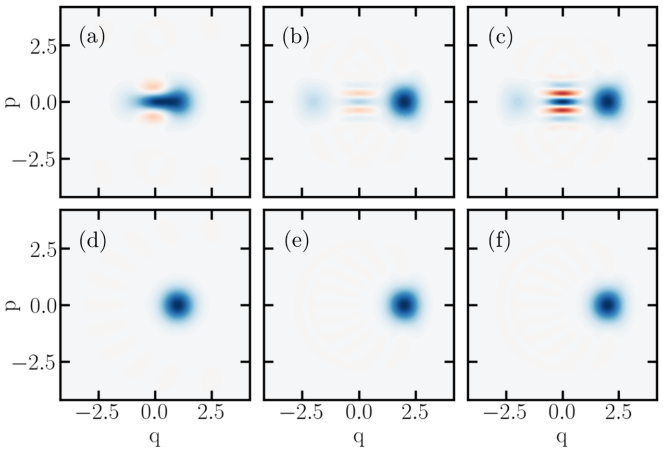

FIG. 9. This demonstrates the effect of detector imperfections for a 2-CT device using the Wigner distribution. Here (a) is the input cat state with amplitude $\alpha = 1$ and unbalanced components $\mathbf{c} = [1.0, 2.0]$. This input cat state is amplified by $g = 2$ gain using a 2-CT device, which produces (b) using 70% efficient detectors or (c) using ideal detectors. The bottom row is similar except using an input coherent state with $\alpha = 1$ amplitude in (d), which produces the output state in (e) using 70% efficient detectors or in (f) using ideal detectors.

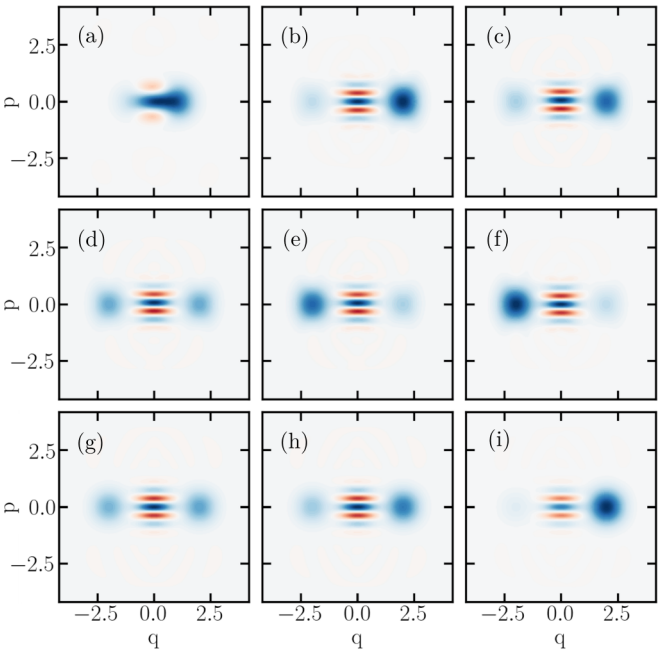

FIG. 10. This demonstrates the effect of misalignment between the input state and 2-CT device using the Wigner distribution. Here (a) is the expected input cat state with amplitude $\alpha = 1$ and unbalanced components $\mathbf{c} = [1.0, 2.0]$. This input cat state is amplified by $g = 2$ gain using a 2-CT device. The input state is phase misaligned by (b) 0 radians, (c) $\pi/4$ radians, (d) $\pi/2$ radians, (e) $3\pi/4$ radians, or (f) π radians. The input state is amplitude misaligned by a factor of (g) 0.1, (h) 0.5, or (i) 1.5.

can see that despite the misalignment a pure coherent-state superposition is still produced (i.e., interference fringes appear unaffected), however, the weighting of the components change.

The misaligned two-component situation is simple enough that we can directly calculate the output state. Suppose we want to amplify the following two-component coherent-state superposition

$$|\psi_{2,\alpha\delta}\rangle = c_1|-\alpha\delta\rangle + c_2|\alpha\delta\rangle. \tag{E1}$$

Here we have an extra factor $\delta \in \mathbb{C}$, which represents magnitude or phase misalignment relative to the resource cat state. The value $\delta = 1$ is the perfect alignment case. We use the following resource two-component cat state

$$|\phi_{2,\beta}\rangle = \frac{1}{\sqrt{\mathcal{N}}}(|\beta\rangle - |-\beta\rangle), \quad \beta = \alpha\sqrt{1+g^2}. \tag{E2}$$

This resource state is put through the gain controlling beam splitter as

$$\begin{aligned} &B_2[\tau = g^2/(1+g^2)]|0\rangle|\phi_{2,\beta}\rangle \\ &\quad = \frac{1}{\sqrt{\mathcal{N}}}(|-\beta\sqrt{1-\tau}\rangle|\beta\sqrt{\tau}\rangle - |\beta\sqrt{1-\tau}\rangle|-\beta\sqrt{\tau}\rangle) \\ &\quad = \frac{1}{\sqrt{\mathcal{N}}}(|-\alpha\rangle|g\alpha\rangle - |\alpha\rangle|-g\alpha\rangle). \end{aligned} \tag{E3}$$

One arm of this state is then mixed with input state on a balanced beam splitter $S_{N=2} = B_2(\tau = \frac{1}{2})$ as follows:

$$\begin{aligned} &B_2(\tau = 1/2)|\psi_{2,\alpha\delta}\rangle B_2(g)|0\rangle|\phi_{2,\beta}\rangle \\ &\quad = \frac{1}{\sqrt{\mathcal{N}}}(c_1|(-\alpha\delta-\alpha)/\sqrt{2}\rangle|(-\alpha\delta+\alpha)/\sqrt{2}\rangle|g\alpha\rangle \\ &\qquad - c_1|(-\alpha\delta+\alpha)/\sqrt{2}\rangle|(-\alpha\delta-\alpha)/\sqrt{2}\rangle|-g\alpha\rangle \\ &\qquad + c_2|(\alpha\delta-\alpha)/\sqrt{2}\rangle|(\alpha\delta+\alpha)/\sqrt{2}\rangle|g\alpha\rangle \\ &\qquad - c_2|(\alpha\delta+\alpha)/\sqrt{2}\rangle|(\alpha\delta-\alpha)/\sqrt{2}\rangle|-g\alpha\rangle). \end{aligned} \tag{E4}$$

Finally, we postselection on $\langle 0|\langle 1|$ to produce the following output state:

$$\begin{aligned} &\langle 0|\langle 1|B_2(\tau = 1/2)|\psi_{2,\alpha\delta}\rangle B_2(g)|0\rangle|\phi_{2,\beta}\rangle \\ &\quad = \frac{e^{-\frac{|\alpha|^2+|\alpha\delta|^2}{2}}}{\sqrt{\mathcal{N}}}\left(c_1\frac{-\alpha\delta+\alpha}{\sqrt{2}}|g\alpha\rangle - c_1\frac{-\alpha\delta-\alpha}{\sqrt{2}}\right. \\ &\qquad \left.\times|-g\alpha\rangle + c_2\frac{\alpha\delta+\alpha}{\sqrt{2}}|g\alpha\rangle - c_2\frac{\alpha\delta-\alpha}{\sqrt{2}}|-g\alpha\rangle\right) \\ &\quad \propto [c_1(1+\delta) + c_2(1-\delta)]|-g\alpha\rangle \\ &\qquad + [c_1(1-\delta) + c_2(1+\delta)]|g\alpha\rangle. \end{aligned} \tag{E5}$$

This expression shows us that the resultant output state will always be a pure coherent-state superposition (i.e., fringes will be maintained), irrespective of the misalignment. However, this misalignment factor δ does have an effect on the output state component weightings.

Let us first consider $\delta = e^{i\phi}$, where ϕ is the input state's phase misalignment from the resource cat state. We can see that with no phase misalignment $\phi = 0 \Rightarrow \delta = 1$, then our expression is the expected output state $c_1|-g\alpha\rangle + c_2|g\alpha\rangle$, which is consistent with the numerical simulation in Fig. 10(b). If there is π-phase misalignment $\phi = \pi \Rightarrow \delta = -1$, this expression reduces down to $c_2|-g\alpha\rangle + c_1|g\alpha\rangle$,

which is consistent with Fig. 10(f). If there is $\pi/2$ misalignment $\phi = \pi/2 \Rightarrow \delta = i$ this expression becomes proportional to $(ic_1 + c_2)|-g\alpha\delta\rangle + (c_1 + ic_2)|g\alpha\delta\rangle$ using the identity $(1+i)/(1-i) = i$; these two components have the same magnitude given c_1 and c_2 are real, which agrees with Fig. 10(d). Finally, consider the effect of decreasing $\delta \to 0$, the output state will tend towards the balanced cat state $|-g\alpha\rangle + |g\alpha\rangle$, which is consistent with our numerical simulations in Figs. 10(g)–10(i).

APPENDIX F: SUCCESS PROBABILITY ANALYSIS

If we assume an arbitrary input state which can be written in the N-components cat basis as in Eq. (1), the unnormalized output state from our N-CT device is given by Eq. (6) as

$$|\psi_{N,g\alpha}\rangle = \frac{e^{-|\alpha|^2}\alpha^{N-1}}{N^{(N-3)/2}\sqrt{\mathcal{N}}}\sum_{a=1}^{N} c_a\left|\omega_N^a g\alpha\right\rangle. \tag{F1}$$

Hence, one can calculate the success probability as

$$\begin{aligned}\mathbb{P} &= \langle\psi_{N,g\alpha}|\psi_{N,g\alpha}\rangle \\ &= \frac{e^{-2|\alpha|^2}|\alpha|^{2(N-1)}}{N^{(N-3)}\mathcal{N}}\sum_{j=1}^{N}\sum_{k=1}^{N} c_j^* c_k e^{(\omega_N^{k-j}-1)|\alpha|^2 g^2}.\end{aligned} \tag{F2}$$

Since two coherent states are not orthogonal $\langle\beta|\alpha\rangle = e^{-(|\beta|^2+|\alpha|^2-2\beta^*\alpha)/2}$, the normalization factor from the cat resource state $|\phi_{N,\beta}\rangle$ can be calculated as

$$\begin{aligned}\mathcal{N} &= \sum_{j,k=1}^{N}\omega_N^{k-j}\langle\omega_N^j\beta|\omega_N^k\beta\rangle \\ &= \sum_{j,k=1}^{N}\omega_N^{k-j}e^{(\omega_N^{k-j}-1)|\beta|^2} \\ &= \sum_{j,k=1}^{N}\omega_N^{k-j}e^{(\omega_N^{k-j}-1)|\alpha|^2(1/\eta+g^2)}.\end{aligned} \tag{F3}$$

Thus, for an N-components input with known coefficients c_a and amplitude α, we can determine the probability for a given gain g and channel transmissivity η.

Now, to gain an idea of how this probability scales, let us consider the coherent-state input case $c_a = \delta_{a,a'}$. The success probability in this case is simply

$$\mathbb{P}_{\rm c} = \frac{e^{-2|\alpha|^2}|\alpha|^{2(N-1)}}{N^{(N-3)}\mathcal{N}}. \tag{F4}$$

We have plotted this equation in Fig. 4. Notice that g^2 and $1/\eta$ act similarly through the factor $\mathcal{N}$. If we increase g or decrease η, then this requires increasing the resource $\beta = \alpha\sqrt{1/\eta + g^2}$. In the large-amplitude limit $\beta \to \infty$ the cat resource $|\phi_{N,\beta}\rangle$ is the sum of N orthogonal states, hence, the normalization factor simply becomes $\mathcal{N} \to N$. In other words,

$$\mathbb{P}_{\rm lim,c} = \lim_{g\to\infty}\mathbb{P}_{\rm c} = \lim_{\eta\to 0}\mathbb{P}_{\rm c} = \frac{e^{-2|\alpha|^2}|\alpha|^{2(N-1)}}{N^{(N-2)}}. \tag{F5}$$

By taking the derivative, we can calculate that the input size

$$\alpha_{\rm max} = \text{argmax}_\alpha\,\mathbb{P}_{\rm lim,c} = \sqrt{(N-1)/2} \tag{F6}$$

maximizes this success probability as

$$\begin{aligned}\mathbb{P}_{\rm max,lim,c} = \max\mathbb{P}_{\rm lim,c} &= \frac{(2e)^{-(N-1)}(N-1)^{N-1}}{N^{(N-2)}} \\ &= \frac{2eN^2}{N-1}\left(\frac{N-1}{2eN}\right)^N.\end{aligned} \tag{F7}$$

Note we may include an additional N factor due to Alice's multiple measurements as explained in Appendix B. Hence, we have shown our N-CT device can teleamplify states with significant success probability in the large gain and/or large loss asymptotic limit. For example, for $N\mathbb{P}_{\rm max,lim,c}(N=2) \approx 0.37$, $N\mathbb{P}_{\rm max,lim,c}(N=3) \approx 0.14$, and $N\mathbb{P}_{\rm max,lim,c}(N=5) \approx 0.01$.

[1] H. Jeong and M. S. Kim, Efficient quantum computation using coherent states, Phys. Rev. A **65**, 042305 (2002).

[2] T. C. Ralph, A. Gilchrist, G. J. Milburn, W. J. Munro, and S. Glancy, Quantum computation with optical coherent states, Phys. Rev. A **68**, 042319 (2003).

[3] A. P. Lund, T. C. Ralph, and H. L. Haselgrove, Fault-Tolerant Linear Optical Quantum Computing with Small-Amplitude Coherent States, Phys. Rev. Lett. **100**, 030503 (2008).

[4] P. Marek and J. Fiurášek, Elementary gates for quantum information with superposed coherent states, Phys. Rev. A **82**, 014304 (2010).

[5] M. Mirrahimi, Z. Leghtas, V. V. Albert, S. Touzard, R. J. Schoelkopf, L. Jiang, and M. H. Devoret, Dynamically protected cat-qubits: A new paradigm for universal quantum computation, New J. Phys. **16**, 045014 (2014).

[6] W. J. Munro, K. Nemoto, G. J. Milburn, and S. L. Braunstein, Weak-force detection with superposed coherent states, Phys. Rev. A **66**, 023819 (2002).

[7] A. Gilchrist, K. Nemoto, W. J. Munro, T. C. Ralph, S. Glancy, S. L. Braunstein, and G. J. Milburn, Schrödinger cats and their power for quantum information processing, J. Opt. B: Quantum Semiclassical Opt. **6**, S828 (2004).

[8] J. Joo, W. J. Munro, and T. P. Spiller, Quantum Metrology with Entangled Coherent States, Phys. Rev. Lett. **107**, 083601 (2011).

[9] Y. M. Zhang, X. W. Li, W. Yang, and G. R. Jin, Quantum fisher information of entangled coherent states in the presence of photon loss, Phys. Rev. A **88**, 043832 (2013).

[10] M. G. Genoni and T. Tufarelli, Non-orthogonal bases for quantum metrology, J. Phys. A: Math. Theor. **52**, 434002 (2019).

[11] N. Sangouard, C. Simon, N. Gisin, J. Laurat, R. Tualle-Brouri, and P. Grangier, Quantum repeaters with entangled coherent states, J. Opt. Soc. Am. B **27**, A137 (2010).

[12] J. B. Brask, I. Rigas, E. S. Polzik, U. L. Andersen, and A. S. Sørensen, Hybrid Long-Distance Entanglement Distribution Protocol, Phys. Rev. Lett. **105**, 160501 (2010).

[13] H.-L. Yin, W.-F. Cao, Y. Fu, Y.-L. Tang, Y. Liu, T.-Y. Chen, and Z.-B. Chen, Long-distance measurement-device-independent quantum key distribution with coherent-state superpositions, Opt. Lett. **39**, 5451 (2014).

[14] H.-L. Yin and Z.-B. Chen, Coherent-state-based twin-field quantum key distribution, Sci. Rep. **9**, 14918 (2019).

[15] A. Zavatta, J. Fiurášek, and M. Bellini, A high-fidelity noiseless amplifier for quantum light states, Nat. Photonics **5**, 52 (2011).

[16] J. Fiurášek, Engineering quantum operations on traveling light beams by multiple photon addition and subtraction, Phys. Rev. A **80**, 053822 (2009).

[17] P. Marek and R. Filip, Coherent-state phase concentration by quantum probabilistic amplification, Phys. Rev. A **81**, 022302 (2010).

[18] N. A. McMahon, A. P. Lund, and T. C. Ralph, Optimal architecture for a nondeterministic noiseless linear amplifier, Phys. Rev. A **89**, 023846 (2014).

[19] J. Zhao, J. Y. Haw, T. Symul, P. K. Lam, and S. M. Assad, Characterization of a measurement-based noiseless linear amplifier and its applications, Phys. Rev. A **96**, 012319 (2017).

[20] S. Zhang and X. Zhang, Photon catalysis acting as noiseless linear amplification and its application in coherence enhancement, Phys. Rev. A **97**, 043830 (2018).

[21] L. Hu, M. Al-amri, Z. Liao, and M. S. Zubairy, Entanglement improvement via a quantum scissor in a realistic environment, Phys. Rev. A **100**, 052322 (2019).

[22] J. Fiurášek, Teleportation-based noiseless quantum amplification of coherent states of light, Opt. Express **30**, 1466 (2022).

[23] B. Yurke and D. Stoler, Generating Quantum Mechanical Superpositions of Macroscopically Distinguishable States Via Amplitude Dispersion, Phys. Rev. Lett. **57**, 13 (1986).

[24] R. Y. Teh, P. D. Drummond, and M. D. Reid, Overcoming decoherence of schrödinger cat states formed in a cavity using squeezed-state inputs, Phys. Rev. Res. **2**, 043387 (2020).

[25] W. K. Wootters and W. H. Zurek, A single quantum cannot be cloned, Nature (London) **299**, 802 (1982).

[26] E. Schrödinger, Die gegenwärtige situation in der quantenmechanik, Naturwissenschaften **23**, 807 (1935).

[27] A. P. Lund, H. Jeong, T. C. Ralph, and M. S. Kim, Conditional production of superpositions of coherent states with inefficient photon detection, Phys. Rev. A **70**, 020101(R) (2004).

[28] A. Ourjoumtsev, R. Tualle-Brouri, J. Laurat, and P. Grangier, Generating optical Schrödinger kittens for quantum information processing, Science **312**, 83 (2006).

[29] S. Glancy and H. M. de Vasconcelos, Methods for producing optical coherent state superpositions, J. Opt. Soc. Am. B **25**, 712 (2008).

[30] T. Gerrits, S. Glancy, T. S. Clement, B. Calkins, A. E. Lita, A. J. Miller, A. L. Migdall, S. W. Nam, R. P. Mirin, and E. Knill, Generation of optical coherent-state superpositions by number-resolved photon subtraction from the squeezed vacuum, Phys. Rev. A **82**, 031802(R) (2010).

[31] K. Huang, H. Le Jeannic, J. Ruaudel, V. B. Verma, M. D. Shaw, F. Marsili, S. W. Nam, E. Wu, H. Zeng, Y. C. Jeong, R. Filip, O. Morin, and J. Laurat, Optical Synthesis of Large-Amplitude Squeezed Coherent-State Superpositions with Minimal Resources, Phys. Rev. Lett. **115**, 023602 (2015).

[32] J. S. Neergaard-Nielsen, Y. Eto, C.-W. Lee, H. Jeong, and M. Sasaki, Quantum tele-amplification with a continuous-variable superposition state, Nat. Photonics **7**, 439 (2013).

[33] T. Hirano, H. Yamanaka, M. Ashikaga, T. Konishi, and R. Namiki, Quantum cryptography using pulsed homodyne detection, Phys. Rev. A **68**, 042331 (2003).

[34] A. Leverrier and P. Grangier, Unconditional Security Proof of Long-Distance Continuous-Variable Quantum Key Distribution with Discrete Modulation, Phys. Rev. Lett. **102**, 180504 (2009).

[35] J. Janszky, P. Domokos, and P. Adam, Coherent states on a circle and quantum interference, Phys. Rev. A **48**, 2213 (1993).

[36] S. Pandey, Z. Jiang, J. Combes, and C. M. Caves, Quantum limits on probabilistic amplifiers, Phys. Rev. A **88**, 033852 (2013).

[37] D. T. Pegg, L. S. Phillips, and S. M. Barnett, Optical State Truncation by Projection Synthesis, Phys. Rev. Lett. **81**, 1604 (1998).

[38] T. Ralph and A. Lund, Nondeterministic noiseless linear amplification of quantum systems, in *Ninth International Conference on Quantum Communication Measurement and Computing (QCMC)*, AIP Conf. Proc. No. 1110 (American Institute of Physics, Melville, NY, 2009), pp. 155–160.

[39] G.-Y. Xiang, T. C. Ralph, A. P. Lund, N. Walk, and G. J. Pryde, Heralded noiseless linear amplification and distillation of entanglement, Nat. Photonics **4**, 316 (2010).

[40] M. S. Winnel, N. Hosseinidehaj, and T. C. Ralph, Generalized quantum scissors for noiseless linear amplification, Phys. Rev. A **102**, 063715 (2020).

[41] J. J. Guanzon, M. S. Winnel, A. P. Lund, and T. C. Ralph, Ideal Quantum Teleamplification up to a Selected Energy Cutoff Using Linear Optics, Phys. Rev. Lett. **128**, 160501 (2022).

[42] J. Fiurášek, Optimal linear-optical noiseless quantum amplifiers driven by auxiliary multiphoton fock states, Phys. Rev. A **105**, 062425 (2022).

[43] W. Zhong, Y.-P. Li, Y.-B. Sheng, and L. Zhou, Quantum scissors for noiseless linear amplification of polarization-frequency hyper-encoded coherent state, Europhys. Lett. **140**, 18003 (2022).

[44] A. Ourjoumtsev, H. Jeong, R. Tualle-Brouri, and P. Grangier, Generation of optical "Schrödinger cats" from photon number states, Nature (London) **448**, 784 (2007).

[45] H. Takahashi, K. Wakui, S. Suzuki, M. Takeoka, K. Hayasaka, A. Furusawa, and M. Sasaki, Generation of Large-Amplitude Coherent-State Superposition via Ancilla-Assisted Photon Subtraction, Phys. Rev. Lett. **101**, 233605 (2008).

[46] M. Takeoka, H. Takahashi, and M. Sasaki, Large-amplitude coherent-state superposition generated by a time-separated two-photon subtraction from a continuous-wave squeezed vacuum, Phys. Rev. A **77**, 062315 (2008).

[47] D. V. Sychev, A. E. Ulanov, A. A. Pushkina, M. W. Richards, I. A. Fedorov, and A. I. Lvovsky, Enlargement of optical schrödinger's cat states, Nat. Photonics **11**, 379 (2017).

[48] B. Vlastakis, G. Kirchmair, Z. Leghtas, S. E. Nigg, L. Frunzio, S. M. Girvin, M. Mirrahimi, M. H. Devoret, and R. J. Schoelkopf, Deterministically encoding quantum information using 100-photon Schrödinger cat states, Science **342**, 607 (2013).

[49] G. Kirchmair, B. Vlastakis, Z. Leghtas, S. E. Nigg, H. Paik, E. Ginossar, M. Mirrahimi, L. Frunzio, S. M. Girvin, and R. J. Schoelkopf, Observation of quantum state collapse and revival due to the single-photon kerr effect, Nature (London) **495**, 205 (2013).

[50] J. Janszky, P. Domokos, S. Szabó, and P. Adám, Quantum-state engineering via discrete coherent-state superpositions, Phys. Rev. A **51**, 4191 (1995).

[51] R. Nair, B. J. Yen, S. Guha, J. H. Shapiro, and S. Pirandola, Symmetric m-ary phase discrimination using quantum-optical probe states, Phys. Rev. A **86**, 022306 (2012).

[52] F. Becerra, J. Fan, G. Baumgartner, J. Goldhar, J. Kosloski, and A. Migdall, Experimental demonstration of a receiver beating the standard quantum limit for multiple nonorthogonal state discrimination, Nat. Photonics **7**, 147 (2013).

[53] C. H. Bennett, Quantum Cryptography Using Any Two Nonorthogonal States, Phys. Rev. Lett. **68**, 3121 (1992).

[54] M. Koashi, Unconditional Security of Coherent-State Quantum Key Distribution with a Strong Phase-Reference Pulse, Phys. Rev. Lett. **93**, 120501 (2004).

[55] K. Tamaki, N. Lütkenhaus, M. Koashi, and J. Batuwantudawe, Unconditional security of the bennett 1992 quantum-key-distribution scheme with a strong reference pulse, Phys. Rev. A **80**, 032302 (2009).

[56] C. H. Bennett and G. Brassard, Quantum cryptography: Public key distribution and coin tossing, Theor. Comput. Sci. **560**, 7 (2014).

[57] H.-K. Lo and J. Preskill, Security of quantum key distribution using weak coherent states with nonrandom phases, Quantum Inf. Comput. **7**, 431 (2007).

[58] K. Brádler and C. Weedbrook, Security proof of continuous-variable quantum key distribution using three coherent states, Phys. Rev. A **97**, 022310 (2018).

[59] D. Sych and G. Leuchs, Coherent state quantum key distribution with multi letter phase-shift keying, New J. Phys. **12**, 053019 (2010).

[60] S. Pirandola, R. Laurenza, C. Ottaviani, and L. Banchi, Fundamental limits of repeaterless quantum communications, Nat. Commun. **8**, 15043 (2017).

[61] M. Lucamarini, Z. L. Yuan, J. F. Dynes, and A. J. Shields, Overcoming the rate–distance limit of quantum key distribution without quantum repeaters, Nature (London) **557**, 400 (2018).

[62] M. S. Winnel, J. J. Guanzon, N. Hosseinidehaj, and T. C. Ralph, Overcoming the repeaterless bound in continuous-variable quantum communication without quantum memories, arXiv:2105.03586.

[63] C. H. Bennett, D. P. DiVincenzo, J. A. Smolin, and W. K. Wootters, Mixed-state entanglement and quantum error correction, Phys. Rev. A **54**, 3824 (1996).

[64] M. M. Wolf, G. Giedke, O. Krüger, R. F. Werner, and J. I. Cirac, Gaussian entanglement of formation, Phys. Rev. A **69**, 052320 (2004).

[65] P. Marian and T. A. Marian, Entanglement of Formation for an Arbitrary Two-Mode Gaussian State, Phys. Rev. Lett. **101**, 220403 (2008).

[66] S. Tserkis and T. C. Ralph, Quantifying entanglement in two-mode gaussian states, Phys. Rev. A **96**, 062338 (2017).

[67] S. Tserkis, S. Onoe, and T. C. Ralph, Quantifying entanglement of formation for two-mode gaussian states: Analytical expressions for upper and lower bounds and numerical estimation of its exact value, Phys. Rev. A **99**, 052337 (2019).

[68] D. V. Reddy, R. R. Nerem, A. E. Lita, S. W. Nam, R. P. Mirin, and V. B. Verma, Exceeding 95% system efficiency within the telecom c-band in superconducting nanowire single photon detectors, in *CLEO: QELS_Fundamental Science* (Optical Society of America, Washington, DC, 2019), p. FF1A–3.

[69] A. E. Lita, A. J. Miller, and S. W. Nam, Counting near-infrared single-photons with 95% efficiency, Opt. Express **16**, 3032 (2008).

[70] F. Marsili, V. B. Verma, J. A. Stern, S. Harrington, A. E. Lita, T. Gerrits, I. Vayshenker, B. Baek, M. D. Shaw, R. P. Mirin *et al.*, Detecting single infrared photons with 93% system efficiency, Nat. Photonics **7**, 210 (2013).

[71] A. J. Miller, S. W. Nam, J. M. Martinis, and A. V. Sergienko, Demonstration of a low-noise near-infrared photon counter with multiphoton discrimination, Appl. Phys. Lett. **83**, 791 (2003).

[72] See https://github.com/JGuanzon/cat-teleamplifier for the *N*-CT simulation code and generated data which can recreate the graphs in this paper. This uses the Strawberry Fields python library, which includes Refs. [77–79].

[73] T. Ralph, P. Lam, and R. Polkinghorne, Characterizing teleportation in optics, J. Opt. B: Quantum Semiclassical Opt. **1**, 483 (1999).

[74] M. Bina, A. Mandarino, S. Olivares, and M. G. A. Paris, Drawbacks of the use of fidelity to assess quantum resources, Phys. Rev. A **89**, 012305 (2014).

[75] A. Mandarino, M. Bina, C. Porto, S. Cialdi, S. Olivares, and M. G. A. Paris, Assessing the significance of fidelity as a figure of merit in quantum state reconstruction of discrete and continuous-variable systems, Phys. Rev. A **93**, 062118 (2016).

[76] S. Tserkis, J. Dias, and T. C. Ralph, Simulation of gaussian channels via teleportation and error correction of gaussian states, Phys. Rev. A **98**, 052335 (2018).

[77] N. Killoran, J. Izaac, N. Quesada, V. Bergholm, M. Amy, and C. Weedbrook, Strawberry fields: A software platform for photonic quantum computing, Quantum **3**, 129 (2019).

[78] T. R. Bromley, J. M. Arrazola, S. Jahangiri, J. Izaac, N. Quesada, A. D. Gran, M. Schuld, J. Swinarton, Z. Zabaneh, and N. Killoran, Applications of near-term photonic quantum computers: software and algorithms, Quantum Sci. Technol. **5**, 034010 (2020).

[79] J. E. Bourassa, N. Quesada, I. Tzitrin, A. Száva, T. Isacsson, J. Izaac, K. K. Sabapathy, G. Dauphinais, and I. Dhand, Fast simulation of bosonic qubits via gaussian functions in phase space, PRX Quantum **2**, 040315 (2021).